Biophysical Chemistry 146 (2010) 118–125

Contents lists available at ScienceDirect

Biophysical Chemistry

journal homepage: http://www.elsevier.com/locate/biophyschem

Arginine 15 stabilizes an S_NAr reaction transition state and the binding of anionic ligands at the active site of human glutathione transferase A1-1

Samantha Gildenhuys [a], Marina Dobreva [a], Nichole Kinsley [a], Yasien Sayed [a], Jonathan Burke [a], Stephen Pelly [b], Graeme P. Gordon [a], Muhammed Sayed [c], Trevor Sewell [d], Heini W. Dirr [a,*]

[a] Protein Structure–Function Research Unit, School of Molecular and Cell Biology, University of the Witwatersrand, Johannesburg 2050, South Africa
[b] Molecular Sciences Institute, School of Chemistry, University of the Witwatersrand, Johannesburg 2050, South Africa
[c] Department of Biotechnology, University of the Western Cape, Bellville 7535, South Africa
[d] Electron Microscope Unit, University of Cape Town, Rondebosch 7701, South Africa

ARTICLE INFO

Article history:
Received 16 October 2009
Received in revised form 12 November 2009
Accepted 12 November 2009
Available online 18 November 2009

Keywords:
Glutathione transferases
Crystal structure
Molecular docking
Isothermal titration calorimetry
Transition state stabilization
Anionic ligand binding

ABSTRACT

Arg15, conserved in class Alpha GSTs (glutathione transferases), is located at the interface between the G- and H-sites of the active site where its cationic guanidinium group might play a role in catalysis and ligand binding. Arg15 in human GSTA1-1 was replaced with a leucine and crystallographic, spectroscopic, thermodynamic and molecular docking methods were used to investigate the contribution made by Arg15 towards (i) the binding of glutathione (GSH) to the G-site, (ii) the pK_a of the thiol group of GSH, (iii) the stabilization of an analog of the anionic transition state of the S_NAr reaction between 1-chloro-2,4-dinitrobenzene (CDNB) and GSH, and, (iv) the binding of the anionic non-substrate ligand 8-anilino-1-naphthalene sulphonate (ANS) to the H-site. While the R15L mutation substantially diminishes the CDNB–GSH conjugating activity of the enzyme, it has little effect on protein structure and stability. Arg15 does not contribute significantly towards the enzyme's affinity for GSH but does determine the reactivity of GSH by reducing the thiol's pK_a from 7.6 to 6.6. The anionic σ-complex formed between GSH and 1,3,5-trinitrobenzene is stabilized by Arg15, suggesting that it also stabilizes the transition state formed in the S_NAr reaction between GSH and CDNB. The trinitrocyclohexadienate moiety of the σ-complex binds the H-site where the catalytic residue, Tyr9, was identified to hydrogen bond to an *o*-nitro group of the σ-complex. The affinity for ANS at the H-site is decreased about 3-fold by the R15L mutation implicating the positive electrostatic potential of Arg15 in securing the organic anion at this site.

© 2009 Elsevier B.V. All rights reserved.

1. Introduction

The canonical cytosolic glutathione transferases (GSTs) are a large superfamily of dimeric enzymes involved in the metabolism of xenobiotic compounds by conjugating them to reduced glutathione (GSH) in preparation for their elimination via the mercapturate pathway [1,2]. The active site on each subunit has two adjacent sites; a GSH-binding site (G-site) and a hydrophobic site for binding nonpolar electrophilic substrates (H-site) [3]. While the binding of GSH to the G-site is conserved in GSTs and is highly specific towards the thiol substrate, the H-site is capable of binding a wide range of structurally diverse electrophilic compounds. A fundamental event in the catalytic mechanism of GSTs is the deprotonation of the thiol group of GSH to form the GS^- anion. In many GSTs, this event is facilitated by either a tyrosine or a serine residue [1,2]. The nucleophilic GS^- anion then reacts with an aromatic electrophilic substrate (e.g., the most widely used substrate CDNB [4]) through an S_NAr reaction that proceeds via a high-energy anionic transition state referred to as a Meisenheimer or σ-complex [5,6]. The structural basis for the binding and stabilization of the transition state has been reported for class Mu and Pi GSTs which have a transition state analog, 1-*S*-(glutathionyl)-2,4,6-trinitrocyclohexadienate, bound at their active sites [7–9]. Crystallographic data indicate the involvement of a pair of topologically equivalent tyrosine residues (Tyr6 and Tyr115 in class Mu and Tyr7 and Tyr108 in class Pi) in catalysis through transition state stabilization via hydrogen bonding. Very little, however, is known about the residues involved in the binding of the transition state to class Alpha GSTs.

In addition to their catalytic functions, GSTs can bind a wide variety of non-substrate ligands many of which are organic anions (e.g., ANS) [10]. This ligandin function is known to result in the inhibition of catalytic function, due to the binding of non-substrates to the promiscuous H-site of GSTs ([11] and references therein). However, the residues involved in binding these ligands are unknown.

Abbreviations: ANS, 8-anilino-1-naphthalene sulphonate; CDNB, 1-chloro-2,4-dinitrobenzene; DTT, dithiothreitol; ITC, isothermal titration calorimetry; GSH, reduced glutathione; GSO_3, glutathione sulphonate; GST, glutathione transferase; GTX, *S*-hexylglutathione; PEG, poly(ethylene glycol); TNB, 1,3,5-trinitrobenzene.

* Corresponding author. Tel.: +27 11 717 6352; fax: +27 11 717 6351.
E-mail address: heinrich.dirr@wits.ac.za (H.W. Dirr).

0301-4622/$ – see front matter © 2009 Elsevier B.V. All rights reserved.
doi:10.1016/j.bpc.2009.11.003

Class Alpha GSTs, major detoxication enzymes and ligand-binding proteins in the liver, have a conserved arginine residue (Arg15) located at the interface between the G- and H-sites. It has been proposed that Arg15 is involved in the binding of GSH via hydrogen bonding and in stabilizing the thiolate form of the tripeptide at the G-site [12], and in binding the anionic non-substrate ligand ANS at the H-site [13] of GSTA1-1. Arg15 is also involved in a salt bridge interaction across the interface between domains 1 and 2 [14]. In the present study, we have used crystallographic, spectroscopic, thermodynamic and molecular docking methods to investigate the contributions made by Arg15 in human GSTA1-1 towards stability, catalysis and ligand binding. Arg15 was replaced with a leucine residue and the wild-type and R15L mutant enzymes studied with respect to their conformational stability, the binding of GSH and its oxidized analog GSO_3 to the G-site, the deprotonation and pK_a of GSH at the G-site, the formation and stabilization of the anionic transition state analog 1-*S*-(glutathionyl)-2,4,6-trinitrocyclohexadienate at the active site, and the binding of the anionic non-substrate ligand ANS to the H-site. Arg15 was replaced with a leucine in order to remove the cationic moiety and maintain most of the bulk. A leucine residue is accommodated at this position in the GST fold as shown for class Mu GSTs.

2. Experimental

2.1. Mutagenesis, expression and purification

The pKHA1 plasmid encoding cDNA sequence for the wild-type hGSTA1-1 was a gift from Prof. B. Mannervik (Uppsala University, Uppsala, Sweden; [15]) and was used as a template for mutagenesis to create the R15L mutant by the QuikChange™ site-directed mutagenesis method (Stratagene, La Jolla, CA). The replacement of the arginine AGA codon with the leucine TTA codon was confirmed by sequencing (Inqaba Biotechnical Industries (Pty) Ltd., Pretoria, South Africa). Wild-type and R15L hGSTA1-1 were over-expressed in BL21 (DE3) *Escherichia coli* cells by IPTG induction and purified using CM-Sepharose chromatography [16]. The column was pre-equilibrated with 10 mM sodium phosphate buffer, 1 mM EDTA, and 0.02% sodium azide, pH 7.0, and the bound protein was eluted with a 0–0.3 M sodium chloride gradient. Following buffer-exchange into 20 mM sodium phosphate, 100 mM sodium chloride, 1 mM EDTA, and 0.02% sodium azide, pH 6.5, protein purity was assessed by SDS-PAGE and the concentration was determined spectrophotometrically at 280 nm using a molar extinction coefficient of 38,200 $M^{-1}\,cm^{-1}$ for both wild-type and R15L hGSTA1-1 [17].

2.2. Crystallization, X-ray detection and data processing

R15L hGSTA1-1 crystals were grown at 298 K using the hanging drop vapor diffusion method. Each 4 μl drop comprised 2 μl of 14 mg/ml of R15L hGSTA1-1 in 0.1 M Tris–HCl, pH 7.5, 10 mM DTT, 0.02% sodium azide solution and 2 μl of the reservoir buffer (5 mM *S*-hexylglutathione, 0.1 M Tris–HCl, pH 7.5, 10 mM DTT, 5–30% PEG 2000 or 4000). The drops were equilibrated against 1 ml of reservoir buffer in sealed wells of Linbro 24-well microplates. Crystals were grown for 3 days, then harvested and soaked briefly in reservoir buffer before mounting on a cryoloop (Hampton Research). X-ray data were collected on a Rigaku RUH3R copper rotating anode X-ray source set at 40 kV and 22 mA with the crystal-detector distance set to 100 mm. Crystals were cooled with an X-stream 2000 low-temperature system. Diffraction data were recorded at 113 K on a Rigaku R-axis IV+ image plate camera with an X-stream 2000 low-temperature system and an AXCO PX50 glass capillary optic system. Images were collected covering an oscillation angle of 0.5° per image. Data were processed using the software packages DENZO [18] and merged and scaled with SCALEPAK [18].

2.3. Structure determination

The structure of R15L hGSTA1-1 complexed with *S*-hexylglutathione was solved by the molecular replacement method using CCP4 software [19]. A phasing model was constructed by removing the water molecules, the Arg15 side chains and the *S*-hexylglutathione ligand coordinates from the 1K3L.pdb wild-type hGSTA1-1 structure [20]. Phasing was done with MOLREP [21] yielding an *R*-factor of 0.387 and a correlation coefficient of 0.607. Model refinement was done with REFMAC5 [22] and model building performed with O [23]. O was also used to build in the Leu15 side chains. After refinement of the ligand-free protein, the model of *S*-hexylglutathione from 1K3L was built into the R15L structure using SwissProt Deep Viewer [24]. Solvent molecules were added using COOT [25]. The final model gave an *R*-factor of 19.2 and *R*-free of 25.9. The final refinement statistics are given in Table 1. Stereochemical validation of the model was performed using PROCHECK [26].

2.4. Spectroscopic methods

Fluorescence emission spectra were measured at 20 °C on a Perkin Elmer LS50B luminescence spectrometer with the excitation and emission bandwidths set at 4 nm and emission spectra collected at a scan rate of 200 nm/min. All spectra were corrected for buffer (in a 20 mM sodium phosphate buffer, pH 6.5, containing 1 mM EDTA and 0.02% sodium azide). Tryptophan residues in the proteins were selectively excited at 295 nm and the emission monitored from 300 nm to 450 nm. When ANS was present with protein, fluorescence resonance energy transfer from tryptophan to ANS was determined by monitoring the emission from 300 nm to 550 nm.

Far-UV CD measurements were conducted at 20 °C using a Jasco model 810 CD spectropolarimeter. CD signals in millidegree ellipticity were converted to mean residue ellipticity $[\Theta]$ (deg $cm^2\,dmol^{-1}$) according to:

$$[\Theta] = 100\,(\text{signal})\,/\,Cnl \qquad (1)$$

where *C* is the concentration of protein in mM, *n* is the number of amino acid residues in the polypeptide chain and *l* is the pathlength in cm.

2.5. Determination of the pK_a of the thiol group of enzyme-bound GSH

Absorbance spectra were recorded from 230 nm to 310 nm on a Jasco V-550 UV–VIS spectrophotometer at 20 °C for 2 mM GSH and

Table 1
Crystallographic data collection and refinement statistics for R15L hGSTA1-1.

PDB code	2R3X
Space group	C121
Unit-cell dimensions	
a (Å)	99.103
b (Å)	93.858
c (Å)	51.566
Resolution ranges (Å)	19.68–1.80
Unique reflections	43444
Completeness (%)	89.9 (85.0)
$I/\sigma(I)$	7.4 (1.0)
R_{fac} (%)	19.2
R_{free} (%)	25.9
Protein atoms	3572
Water molecules	616
Average *B*-value (Å^2)	18.38
r.m.s. deviations in bond length (Å)	0.017
r.m.s. deviations in bond angles (Å)	1.508
Residues in most allowed regions of Ramachandran plot (%)	93.4
Overall average *G*-factor	0.13
Asymmetric unit content	Dimer

R_{free} was calculated against 5% of the reflections removed at random.
G-factor calculated by PROCHECK.

50 μM R15L hGSTA1-1 (subunit concentration) in 0.1 M sodium phosphate, pH 5.2–9.3. Difference spectra were obtained by subtracting the spectrum for enzyme alone (at pH 5.2) and that for GSH alone at the different pH values from the spectrum of the binary enzyme–GSH complex. The pK_a of the thiol group of enzyme-bound GSH was calculated from a plot of the absorbance at 239 nm versus pH [6,27,28].

2.6. Equilibrium unfolding studies

Equilibrium unfolding studies were conducted as described previously [17]. Protein concentration was 2 μM in urea at 0 M to 8 M in a 20 mM sodium phosphate buffer, pH 6.5, containing 1 mM EDTA and 0.02% sodium azide. Structural changes were monitored by far-UV CD at 222 nm and tryptophan fluorescence at 330 nm. Unfolding data were analyzed according to a two-state model with only folded (N_2) and unfolded (U) states [29].

2.7. Enzyme activity studies

The hGSTA1-1 catalyzed conjugation of CDNB to GSH at 20 °C was monitored spectrophotometrically at 340 nm in 0.1 M sodium phosphate, 1 mM EDTA, pH 6.5, with 1 mM CDNB and 1 mM GSH [30]. Non-enzymatic rates were subtracted from the enzymatic rates.

2.8. Formation of σ-complex between glutathione and 1,3,5-trinitrobenzene

The formation of the σ-complex (1-*S*-(glutathionyl)-2,4,6-trinitrocyclohexadienate) between 5 mM GSH and 0–1000 μM 1,3,5-trinitrobenzene (TNB) was carried out at 20 °C with 20–30 μM enzyme subunits in 0.1 M sodium phosphate buffer, pH 6.5, containing 0.02% sodium azide, essentially as described [6]. The formation constant for the σ-complex, K_f, was determined by non-linear regression analysis of the absorbance data at 450 nm as described previously [31].

2.9. Isothermal titration calorimetry

The energetics of complex formation between R15L hGSTA1-1 and GSH, GSO_3^- or ANS were determined in 20 mM sodium phosphate, 100 mM NaCl, 1 mM EDTA and 0.02% sodium azide, pH 6.5, using a VP-ITC microcalorimeter (MicroCal Inc.) [32]. R15L hGSTA1-1 (69 to 336 μM subunit concentration) in the sample cell was titrated with 3–10 μl aliquots of either 40 mM GSH, 12 mM GSO_3^- or 30.3 mM ANS at 25 °C. For ANS, the temperature range was 5–25 °C. Raw data were integrated, corrected for heats of dilution, and analyzed with ORIGIN v.5. The best fits were obtained for the one-site fitting model giving values for the independent parameters ΔH_{obs}, N and K_a. The parameters ΔS_{obs} and ΔG_{obs} were obtained from $\Delta G = -RT\ln K_a$ and $\Delta G = \Delta H - T\Delta S$ where R is the gas constant and T is the absolute temperature in Kelvin. No correction was made for possible proton-linkage effects occurring during binding. ΔC_p for the binding of ANS to R15L hGSTA1-1 was obtained from the slope of the linear plot of ΔH_{obs} versus temperature.

2.10. Molecular docking

The σ-complex 1-*S*-(glutathionyl)-2,4,6-trinitrocyclohexadienate, an analog of the anionic transition state of the S_NAr reaction between CDNB and GSH, was docked into the crystal structures of wild-type hGSTA1-1 (PDB code 1K3L) and R15L hGSTA1-1 (PDB code 2R3X) using Accelrys Discovery Studio 2.1. A binding sphere with a radius of 7 Å was defined for docking using the location of *S*-hexylglutathione bound to both structures. Docking of the σ-complex to the proteins was conducted using CDocker and the highest scoring pose according to CDocker Energy for each protein structure was then selected. Further energy minimization employing CHARMm was performed to optimize the σ-complex-to-protein interactions which involved a full protein minimization with fixed atom constraints applied to the protein backbone and not the side chains of each structure. A Generalized Born with molecular volume (GBMV) solvation model was employed in the minimization. Models were drawn using PyMOL Molecular Graphics Software (http://pymol.sourceforge.net/).

3. Results and discussion

3.1. Structural properties of R15L hGSTA1-1

Crystals of R15L hGSTA1-1 complexed with *S*-hexylglutathione (GTX) were grown in 15% (w/v) PEG4000, 0.1 M Tris–HCl, pH 7.5, 10 mM DTT, and 0.02% sodium azide, at 20 °C. The electron density of the final model is well defined for residues 2–222 and 4–222 for chains A and B, respectively. Table 1 shows the statistics for the crystallographic data collection and refinement of the R15L hGSTA1-1•*S*-hexylglutathione complex. Fig. 1A shows that the electron density for residue 15 in chains A and B is consistent with a leucine residue at this position. Electron density defining the locations and conformations of *S*-hexylglutathione bound to chains A and B were clear except for the terminal three carbons of the hexyl moiety bound to chain A and the terminal carbon of the hexyl moiety bound to chain B (Fig. 1B). The backbone structures of wild-type hGSTA1-1 (PDB code 1K3L; [20]) and R15L hGSTA1-1 superimpose with an RMSD of 0.27 indicating that the mutation has very little effect on the overall structure of the protein. The hydrogen-bond interactions across the domain interface between Arg15 (domain 1) and Glu104 (domain 2) in the wild-type are disrupted in the R15L structure, and the shorter side chain of Leu15 in the mutant creates a cavity that is filled by three water molecules (Fig. 1C). The hydrogen bonding requirements of Glu104 in the mutant are satisfied by interacting with two of these water molecules (W2 and W3) and with another (W1) found in both mutant and wild-type structures.

The global structure of apo hGSTA1-1 in solution is not perturbed by the R15L mutation, as demonstrated by the overlapping far-UV CD and tryptophan fluorescence spectra for the mutant and wild-type proteins (Fig. S1 in supplementary online data). Furthermore, the loss of the hydrogen bonds across the domain interface in the mutant and the cavity created at the domain interface by truncating the side chain of Arg15 (Fig. 1C), do not destabilize the structure. This is most likely attributed to the involvement of the three ordered water molecules in hydrogen bonding and in improving packing density in lieu of the guanidinium group of Arg15 (Fig. 1C). The thermodynamic parameters of stability, obtained from urea-induced unfolding curves (Fig. S2 in supplementary online data), are similar for both proteins ($\Delta G(H_2O) = 22 \pm 1.74$ kcal mol^{-1}, $m = 3.3 \pm 0.38$ kcal mol^{-1} M^{-1} and $C_m = 4.6$ M urea for R15L, and $\Delta G(H_2O) = 22.6 \pm 1.02$ kcal mol^{-1}, $m = 3.2 \pm 0.22$ kcal mol^{-1} M^{-1} and $C_m = 4.5$ M urea for wild-type.

3.2. Role of Arg15 in the binding and activation of GSH

The specific activity of hGSTA1-1 in conjugating CDNB to GSH (both at 1 mM) is significantly diminished (1.53 μmol/min/mg) when compared to that of the wild-type enzyme (34.9 μmol/min/mg), in agreement with that reported previously [12].

Reduced GSH binds to the G-site of the enzyme in a manner essentially the same as that observed for the GSH moiety of *S*-hexylglutathione shown in Fig. 1B. Although Arg15 forms part of the G-site, the crystal structure of the hGSTA1-1·GSH complex (PDB code 1PKW; [33]) shows that its guanidinium group does not hydrogen bond to the thiol group of GSH (distance>4 Å), as suggested by others [12]. While the K_M for CDNB is not significantly affected when Arg15 is substituted with either a leucine or an isoleucine, the K_M for GSH is

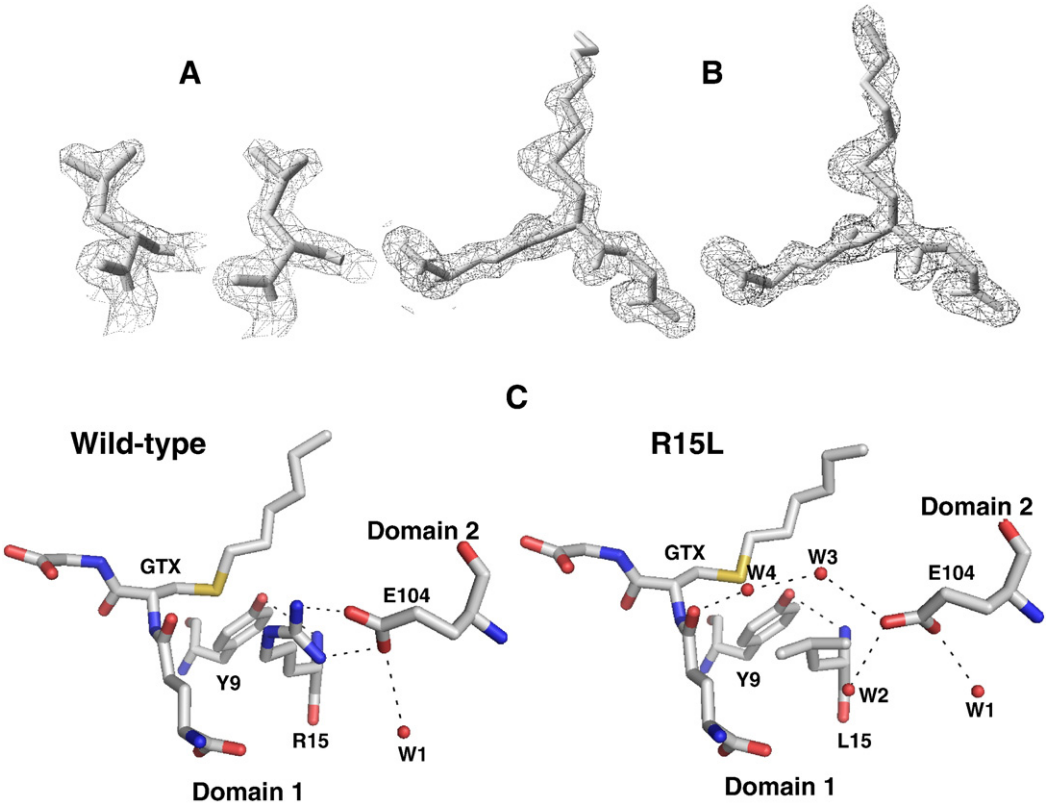

Fig. 1. Electron density maps of R15L hGSTA1-1 (PDB code 2R3X) and active site of GST A1-1. (A) Residue 15 in chain A (right) and in chain B (left) contoured at 2σ. The stick model is that of leucine. (B) *S*-hexylglutathione bound to chain A (right) and bound to chain B (left) contoured at 1.5σ. (C) Stick representations showing bound *S*-hexylglutathione (GTX), amino acids Tyr9, Arg15 (wild-type), Leu15 (R15L) and Glu104. Water molecules are shown as red spheres and hydrogen bonds as dashed lines. Domain 1 and domain 2 are the two structural domains in each subunit with the interactions between Arg15 and Glu104 occurring across the domain interface.

increased 6- to 10-fold [12,34]. Our ITC data at 25 °C indicate that the affinity between GSH and R15L is reduced only 1.31-fold (Table 2; see Fig. S3 in supplementary online data). This suggests that the significant reduction in activity and increase in the K_M for GSH for the R15L mutant are not a consequence of a loss in affinity for GSH, as suggested by others [12]. Arg15 does, however, contribute significantly towards the affinity of the anionic GSH analog, GSO_3^-, as indicated by ITC-determined K_d values (Table 2; see Fig. S4 in supplementary online data). Crystal structures show that the bulkier, negatively charged sulphonate group of GSO_3^- is situated closer to, and hydrogen bonds with, the guanidinium group of Arg15 (PDB codes 1EV4 and 1EV9; [35]).

When GSH binds to the G-site of GSTA1-1, the pK_a of the thiol group is reduced by 2.7 pH units from 9.2 to 6.5 [36], equivalent to a ΔG of −15.4 kJ mol^{-1}. The hydroxyl group of Tyr9 hydrogen bonds to the sulfur atom of GSH [14] facilitating the deprotonation of GSH and, consequently, the formation of the highly nucleophilic GS^- thiolate anion at the active site, a fundamental event in the catalytic mechanism of GSTs. In addition to Tyr9, Arg15, through the positive electrostatic potential generated by its guanidinium group, is also proposed to play an important role in stabilizing the negatively charged thiolate form of GSH [12,34]. This was tested directly by measuring the formation of the thiolate GS^- anion in the R15L mutant E·GSH binary complex. Absorbance data at 239 nm, due to the thiolate anion [37,38], show that the replacement of Arg15 with a leucine residue raises the pK_a of the thiol group to 7.6 in the mutant E·GSH complex (Fig. 2), suggesting that Arg15 contributes about 6 kJ mol^{-1} towards the stabilization of the GS^- anion at the wild-type G-site. Therefore, since the affinity of GSH is not significantly affected by the R15L mutation, the reactivity of GSH bound to the enzyme appears to be an important determinant of the k_{cat} for the GSH/CDNB reaction pathway and, thus, the K_M for GSH. The k_{cat} is lowered to about 3–6% of the wild-type value for the R15I and R15L mutations [12,34]. It has been suggested that Arg15 forms part of an electron-sharing network in class Alpha GSTs that assists in the ionization of GSH at the G-site, and that a similar electrostatic motif is conserved at the G-sites of other GST classes that operates in the "base-assisted deprotonation" model for activating GSH [39,40].

Table 2
Thermodynamic parameters for the binding of GSH and GSO_3^- to wild-type and R15L hGST A1-1 at 25 °C.

	Wild-type		R15L	
	GSH	GSO_3^-	GSH	GSO_3^-
K_d (μM)	351	1.7	460	118
ΔG (kJ mol^{-1})	−19.6	−30.8	−19.0	−22.5
ΔH (kJ mol^{-1})	−19.5	−41.8	−19.2	−59.1
$T\Delta S$ (kJ mol^{-1})	0.9	−11	−0.18	−37
N	1.0	1.0	1.0	0.7

3.3. Role of Arg15 in σ-complex formation

The nucleophilic aromatic substitution, S_NAr, reaction between CDNB and GSH is believed to proceed through a high-energy anionic intermediate, a Meisenheimer or σ-complex [5]. An analog of this transition state can be formed between GSH and 1,3,5-trinitrobenzene (TNB) but, because the hydride ion is a poor leaving group, the reaction with TNB does not proceed to product formation resulting in a dead-end σ-complex (1-(*S*-glutathionyl)-2,4,6-trinitrocyclohexadienate) in equilibrium with the reactants [6,31,41] (Fig. 3A). To establish the role of Arg15 in the formation of this anionic transition state analog at the

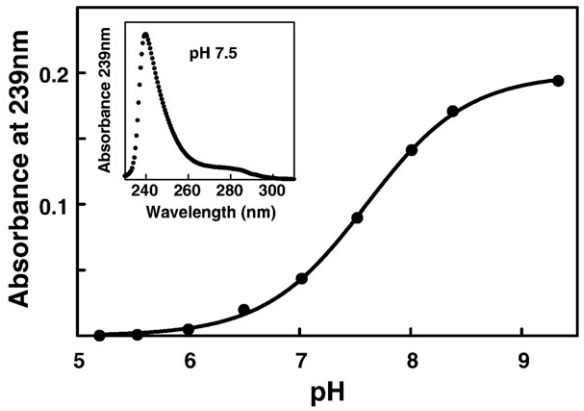

Fig. 2. Ionization of GSH at the G-site of R15L hGSTA1-1. Titration curve of GSH bound to R15L hGSTA1-1 as a function of pH. The ionization of GSH to its thiolate form GS^- was monitored by UV-difference spectroscopy at 239 nm. The inset shows a difference spectrum for the enzyme·GSH complex at pH 7.5. Curve fitting of the data (solid line) yielded a pK_a value of 7.6 for the thiol group of GSH.

active sites of wild-type and R15L hGSTA1-1, the reaction between GSH and TNB was monitored spectroscopically at 450 nm [31,42] (Fig. 3B). The formation constant, K_f, and corresponding A_{max} values for enzyme-bound σ-complex, determined using absorbance values at 450 nm, are $K_f = 7769 \pm 774\ M^{-1}$ and $A_{max} = 11380 \pm 253\ M^{-1}\ cm^{-1}$ for wild-type, and $K_f = 4047 \pm 184\ M^{-1}$ and $A_{max} = 8665 \pm 150\ M^{-1}\ cm^{-1}$ for R15L hGSTA1-1. The K_f value for wild-type compares well with that reported earlier [31]. Assuming that the molar extinction of the σ-complex formed at the active site of hGSTA1-1 is the same as that in solution ($25{,}000\ M^{-1}\ cm^{-1}$) [42], the maximum absorbance values obtained for wild-type and R15L correspond to 46% and 35% σ-complex formed at their active sites at pH 6.5, respectively.

The difference in the free energy change for the formation of the σ-complex ($\Delta\Delta G$), calculated from $\Delta\Delta G = -RT\ln(K_{f\ R15L\ hGSTA1\text{-}1}/K_{f\ wild\text{-}type\ hGSTA1\text{-}1})$, indicates that Arg15 stabilizes the σ-complex at the active site of wild-type hGSTA1-1 by 1.6 kJ mol^{-1}. This value, however, is significantly lower than a $\Delta\Delta G$ of 9.9 kJ mol^{-1} calculated from the k_{cat}/K_M^{CDNB} values for the R15L and wild-type enzymes [12], suggesting that the contribution made by Arg15 towards the catalytic rate in terms of stabilizing the transition state may not be the only major factor for GSTA1-1. The differences between the σ-complex formed with TNB and the actual intermediate formed with CDNB (1-chloro-1-(*S*-glutathionyl)-2,4-trinitrocyclohexadienate) are the presence of an extra *o*-nitro group and the absence of a chlorine leaving group bound to C1 in the trinitrocyclohexadienate moiety. Whether these differences contribute towards the different ΔΔG values for TNB and CDNB is not clear at present.

Since no crystal structure is available for the hGSTA1-1·σ-complex, molecular docking experiments were performed with the σ-complex and both forms of hGSTA1-1. The final energy-minimized models for wild-type and R15L indicate that the GSH moiety of the σ-complex is positioned in essentially the same way as observed for GSH bound at the G-site of hGSTA1-1 (Fig. 4). The trinitrocyclohexadienate moiety fits into the same binding pocket to which the hexyl chain of *S*-hexylglutathione binds. The hydrophobic pocket is formed by the side chains of Tyr9, Phe10, Gly14, Arg15, Leul07, Leu108, Val111, Phe220 and Phe222 (Fig. 4). The latter two residues are located in helix 9 implying that the highly dynamic behavior of this helix [43] is most likely involved in the formation and stabilization of the σ-complex. Further, Phe220 and Phe222 have been shown to play an important role in hGSTA1-1 catalysis with CDNB possibly by modulating the motions of the substrates and steering them into the transition state [44].

In the model of the wild-type·σ-complex, only the *pro-R o*-nitro group of the trinitrocyclohexadienate moiety hydrogen bonds to the

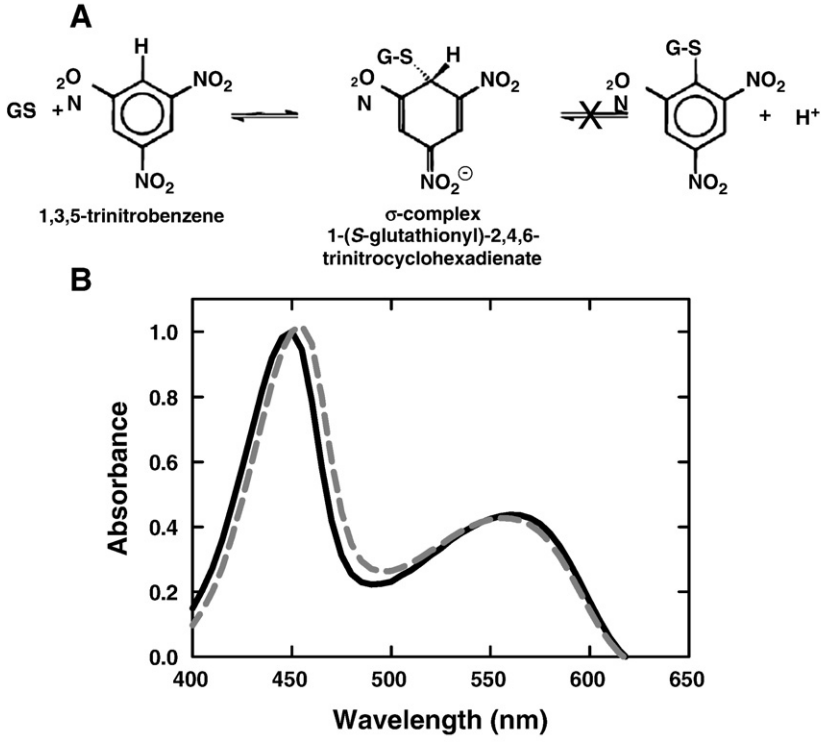

Fig. 3. Formation of the anionic σ-complex at the active site of R15L hGSTA1-1. (A) Reaction between the glutathione thiolate GS^- and trinitrobenzene. The second reaction step does not occur due to the absence of a leaving group on carbon 1 of trinitrobenzene. (B) Difference Vis-spectra of the σ-complex bound to wild-type (solid line) and R15L (dashed line) hGSTA1-1. Spectra were recorded at 20 °C in 0.1 M sodium phosphate buffer, pH 6.5, containing 0.02% sodium azide. GSH was at 5 mM, enzyme subunit concentrations were 20–30 μM and trinitrobenzene was at 0.8 mM.

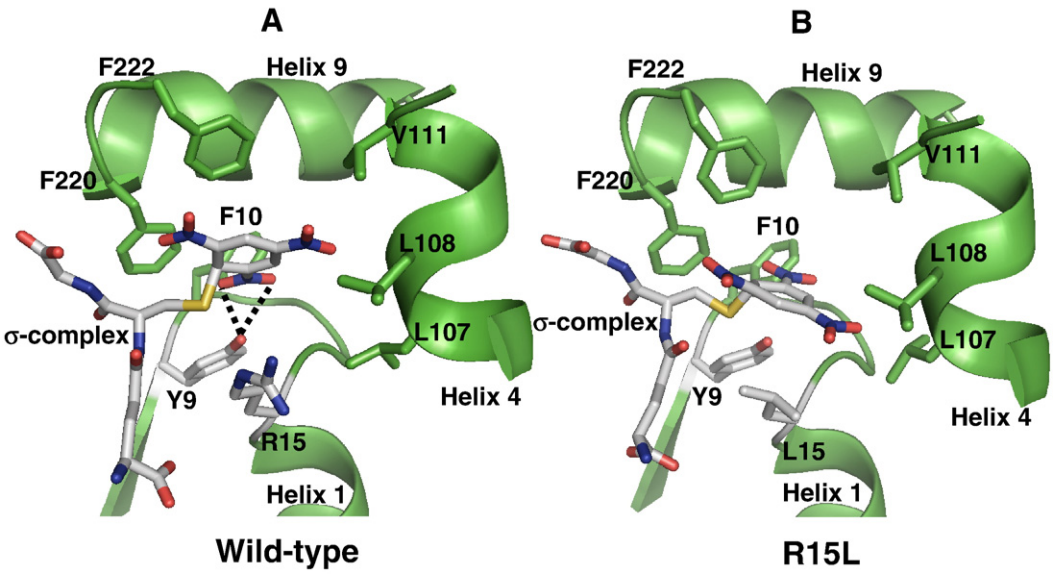

Fig. 4. Model of the anionic σ-complex bound at the active site hGSTA1-1. (A) Wild-type active site with Arg15. (B) R15L active site with Leu15. Stick representations showing bound σ-complex, amino acids Tyr9, Phe10, Arg15 (A), Leu15 (B), Leu107, Leu108, Val111, Phe220 and Phe222. Helices 1, 4 and 9 are indicated by ribbons and hydrogen bonds as dashed lines.

protein via the hydroxyl group of Tyr9 (Fig. 4A). Therefore, in addition to its role in deprotonating the thiol group of glutathione [45], the model implicates Tyr9 in catalysis through transition state stabilization. The proximity of a positive electrostatic potential, generated by both the guanidinium cation of Arg15 and the N-terminus of helix 1, to the trinitrocyclohexadienate moiety may further stabilize the σ-complex. In the R15L·σ-complex, the trinitrocyclohexadienate moiety moves towards the cavity created by the mutation thus eliminating the hydrogen bonding between an *o*-nitro group and Tyr6 (Fig. 4B). Although the pK_a of the hydroxyl group of Tyr9 is reduced in the R15L mutant [12], it would still be protonated at pH 6.5. The position of the trinitrocyclohexadienate moiety in the R15L mutant structure is very similar to that observed for the moiety bound to rGSTM1-1 [7], which has a leucine residue (Leu12) in a position topologically equivalent to Arg15 (Fig. S5 in supplementary online data). Hydrogen bonding is also observed between an *o*-nitro group of the trinitrocyclohexadienate moiety of the σ-complex and the active site tyrosine residue in Mu (Tyr6) [7,8] and in Pi (Tyr7) [9] class GSTs. In these structures, an additional hydrogen bond is formed between the same *o*-nitro group and the hydroxyl group of a topologically equivalent tyrosine residue (Tyr115 in Mu and Tyr107 in Pi) located in the loop between helices 4 and 5 (Fig. S5 in supplementary online data). In hGSTA1-1, the residue is a valine residue (Val111 in Fig. 4). Furthermore, the other *o*-nitro group and the *p*-nitro group of the trinitrocyclohexadienate moiety at the Mu active site are hydrogen bonded to ordered water molecules [7]. When compared to hGSTA1-1, the Mu GST binds the σ-complex significantly more tightly ($K_f = 51{,}000\ M^{-1}$ at pH 7) at its active site [6]. While class Pi GSTP1-1 has an arginine (Arg13) that is topologically equivalent to Arg15 in GSTA1-1, no interactions are observed between its guanidinium group and the trinitrocyclohexadienate moiety of the σ-complex [9].

Spatially, the active site of GSTA1-1 is far more restrictive than that of the GSTM1-1 site due to the presence of helix 9 in the former (Fig. S5 in supplementary online data). In the crystal structure of rGSTM1-1·σ-complex (PDB code 4GST), there is sufficient space to accommodate the chlorine leaving group present in the authentic anionic intermediate (1-chloro-1-(*S*-glutathionyl)-2,4-dinitrocyclohexadienate) and that the chlorine atom is accessible to solvent that would facilitate the decomposition of the intermediate to products [7]. However, according to the model of the hGSTA1-1·σ-complex (Fig. S5 in supplementary online data), the sp^3-hybridized C1 of the authentic intermediate would position the chlorine leaving group close to Phe220 and Phe222 thereby significantly diminishing its accessibility to solvent. However, the dynamic motions of the C-terminal region of the enzyme in catalysis [44] could facilitate the decomposition of the intermediate to products. Unlike that for the class Mu GSTs, formation and decomposition of the Meisenheimer complex in class Alpha GSTs might be rate-limiting for catalysis [46–49].

3.4. Binding of anionic ANS to R15L hGSTA1-1

Molecular docking and ligand-displacement studies indicate the anionic non-substrate ligand ANS to bind the hydrophobic H-site of hGSTA1-1 [13]. The negatively charged sulphonate group of ANS is located at the interface between the G- and H-sites and is in close proximity to Arg15 but does not hydrogen bond to the residue. Fluorescence measurements show that the emission intensity of ANS bound to the R15L mutant is reduced by about one-third when compared to that for the wild-type·ANS complex (Fig. S6 in supplementary online data), suggesting that the mutation reduces the affinity for ANS. The emission maximum wavelength at 475 nm for ANS, however, is unchanged by the mutation suggesting that the hydrophobic nature of the binding site is not compromised.

ITC experiments were conducted to quantify the contribution of Arg15 towards the binding energetic of ANS over the temperature range of 5–25 °C. Binding to R15L hGSTA1-1 is exothermic and the binding data fit well to a model describing one binding site per subunit (Fig. S7 in supplementary online data), consistent with the wild-type data [32]. The affinity of hGSTA1-1 for ANS is diminished 3.3-fold by the R15L mutation ($K_d = 215$ μM for R15L and 65 μM for wild-type [32] at 25 °C), indicating the importance of this residue in the binding of ANS. The temperature dependence of the thermodynamic parameters obtained for the R15L·ANS interaction is presented in Fig. 5. The observed free energy (ΔG_{obs}) remains essentially constant over the 5–25 °C range and is defined by negative favorable enthalpy values (ΔH_{obs}) and positive favorable entropy values ($T\Delta S_{obs}$). The importance of van der Waals contacts between the anilino and naphthyl rings of ANS and protein surface for the enthalpically driven binding of ANS to wild-type hGSTA1-1 and other proteins has been shown [32,50–52]. At 25 °C, the enthalpy change for the R15L protein is less favorable ($\Delta H_{obs} = -18.6$ kJ mol) than that for the wild-type protein ($\Delta H_{obs} = -30.5$ kJ mol),

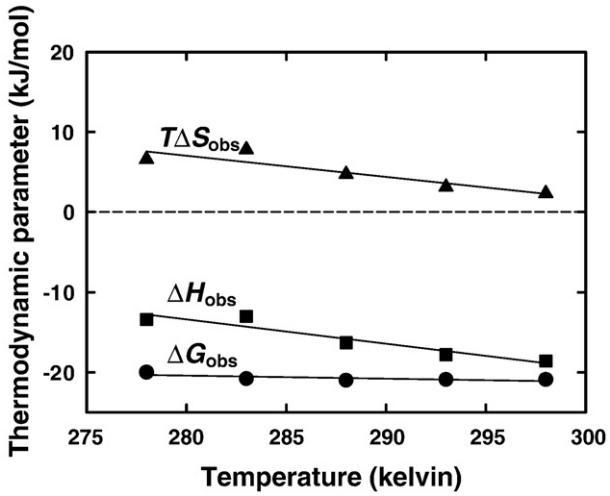

Fig. 5. Calorimetric titration of R15L hGSTA1-1 with the anionic ligand ANS. Temperature dependence of (■)ΔH_{obs}, (▲)$T\Delta S_{obs}$ and (●) ΔG_{obs} for the binding of ANS to R15L hGSTA1-1 in 20 mM sodium phosphate, 1 mM EDTA, and 0.02% sodium azide, pH 6.5. The solid lines represent linear fits to the experimental data.

demonstrating the contribution of electrostatic interactions between the negatively charged sulphonate group of ANS and the positively charged guanidinium group of Arg15. The presence of electrostatic interactions between the sulphonate group of ANS and the guanidinium group of an arginine residue has also been demonstrated for other protein·ANS complexes [50,52–55].

The positive $T\Delta S_{obs}$ value for the R15L mutant (2.3 kJ mol at 25 °C) reflects a net favorable entropy change of solvation in that restrained water molecules solvating, at least, the nonpolar surface of the anilinonaphthalene moiety and negatively charged sulphonate group of free ANS are released to bulk solvent upon complex formation [56]. Free ANS has a relatively constrained conformation with the position of the sulphonate group relative to the anilinonaphthalene moiety being defined by a dihedral angle and a torsion angle [50]. The favorable $T\Delta S_{obs}$ value for the R15L mutant compared to the unfavorable $T\Delta S_{obs}$ value for the wild-type (-6.5 kJ mol [32]) indicates a much smaller unfavorable change in conformational entropy due to a loss of degrees of freedom at the interface between ANS and protein. It is possible that in the absence of the interactions between the sulphonate groups of ANS and Arg15, the conformation of ANS bound to R15L is not as rigid as it would be when bound to the wild-type protein.

The change in heat capacity ($\Delta C_{p,\ obs}$) for the binding of ANS to R15L hGSTA1-1, calculated from the linear temperature dependence of ΔH_{obs} (Fig. 5), is -0.30 kJ mol^{-1} K^{-1} compared to a value of -0.84 kJ mol^{-1} K^{-1} reported for the wild-type hGSTA1-1·ANS interaction [32]. Since the change in heat capacity originates primarily from the changes in the hydration of nonpolar and polar molecular surface areas [57], the negative change observed for the mutant suggests the burial of nonpolar surface area on complex formation [58], consistent with the hydrophobic nature of the binding site and ligand.

Acknowledgements

This work was supported by the University of the Witwatersrand, the South African National Research Foundation Grant 205359 (to H. W. D.), and the South African Research Chairs Initiative of the Department of Science and Technology and National Research Foundation Grant 64788 (to H. W. D.). Any opinion, findings and conclusions or recommendations expressed in this material are those of the author(s) and therefore the NRF and DST do not accept any liability with regard thereto.

Appendix A. Supplementary data

Supplementary data associated with this article can be found, in the online version, at doi:10.1016/j.bpc.2009.11.003.

References

[1] R.N. Armstrong, Structure, catalytic mechanism, and evolution of the glutathione transferases, Chem. Res. Toxicol. 10 (1997) 2–18.
[2] D. Sheehan, G. Meade, V.M. Foley, C.A. Dowd, Structure, function and evolution of glutathione transferases: implications for classification of non-mammalian members of an ancient enzyme superfamily, Biochem. J. 360 (2001) 1–16.
[3] H. Dirr, P. Reinemer, R. Huber, X-ray crystal structure of cytosolic glutathione *S*-transferases. Implications for protein architecture, substrate recognition and catalytic function, Eur. J. Biochem. 220 (1994) 645–661.
[4] W.H. Habig, M.J. Pabst, W.B. Jakoby, Glutathione *S*-transferases. The first enzymatic step in mercapturic acid formation, J. Biol. Chem. 249 (1974) 7130–7139.
[5] C.F. Bernasconi, Mechanisms of nucleophilic aromatic and heteroaromatic substitution. Recent developments, Chimia 34 (1980) 1–11.
[6] G.F. Graminski, P. Zhang, M.A. Sesay, H.L. Ammon, R.N. Armstrong, Formation of the 1-(*S*-glutathionyl)-2, 4, 6-trinitrocyclohexadienate anion at the active site of glutathione *S*-transferase: evidence for enzymic stabilization of σ-complex intermediates in nucleophilic aromatic substitution reactions, Biochemistry 28 (1989) 6252–6258.
[7] X. Ji, R.N. Armstrong, G.L. Gilliland, Snapshots along the reaction coordinate of an S_NAr reaction catalyzed by glutathione transferase, Biochemistry 32 (1993) 12949–12954.
[8] Y. Patskovsky, L. Patskovska, S.C. Almo, I. Listowsky, Transition state model and mechanism of nucleophilic aromatic substitution reactions catalyzed by human glutathione *S*-transferase M1a–1a, Biochemistry 45 (2006) 3852–3862.
[9] L. Prade, R. Huber, T.H. Manoharan, W.E. Fahl, W. Reuter, Structures of class pi glutathione *S*-transferase from human placenta in complex with substrate, transition-state analogue and inhibitor, Structure 5 (1997) 1287–1295.
[10] G. Litwack, B. Ketterer, I.M. Arias, Ligandin: a hepatic protein which binds steroids, bilirubin, carcinogens and a number of exogenous organic anions, Nature (London) 234 (1971) 466–467.
[11] D. Kolobe, Y. Sayed, H.W. Dirr, Characterization of bromosulphophthalein binding to human glutathione *S*-transferase A1-1: thermodynamics and inhibition kinetics, Biochem. J. 382 (2004) 703–709.
[12] R. Björnestedt, G. Stenberg, M. Widersten, P.G. Board, I. Sinning, T.A. Jones, B. Mannervik, Functional significance of arginine 15 in the active site of human class alpha glutathione transferase A1-1, J. Mol. Biol. 247 (1995) 765–773.
[13] H.W. Dirr, T. Little, D.C. Kuhnert, Y. Sayed, A conserved N-capping motif contributes significantly to the stabilization and dynamics of the C-terminal region of class alpha glutathione transferases, J. Biol. Chem. 280 (2005) 19480–19487.
[14] I. Sinning, G.J. Kleywegt, S.W. Cowan, P. Reinemer, H.W. Dirr, R. Huber, G.L. Gilliland, R.N. Armstrong, X. Ji, P.G. Board, B. Olin, B. Mannervik, T.A. Jones, Structure determination and refinement of human alpha class glutathione transferase A1-1, and a comparison with the Mu and Pi class enzymes, J. Mol. Biol. 232 (1993) 192–212.
[15] G. Stenberg, R. Björnestedt, B. Mannervik, Heterologous expression of recombinant human glutathione transferase A1-1 from a hepatoma cell line, Protein. Expr. Purif. 3 (1992) 80–84.
[16] Y. Sayed, L.A. Wallace, H.W. Dirr, The hydrophobic lock-and-key intersubunit motif of glutathione transferase A1-1: implications for catalysis, ligandin function and stability, FEBS Lett. 465 (2000) 169–172.
[17] L.A. Wallace, N. Sluis-Cremer, H.W. Dirr, Equilibrium and kinetic unfolding properties of dimeric human glutathione transferase A1-1, Biochemistry 37 (1998) 5320–5328.
[18] Z. Otwinowski, W. Minor, Processing of X-ray diffraction data collected in oscillation mode, Methods Enzymol. 276 (1997) 307–326.
[19] Collaborative Computational Test article sample title placed here, Acta Crystallogr, D Biol. Crystallogr. D50 (1994) 760–763.
[20] I. Le Trong, R.E. Stenkamp, C. Ibarra, W.M. Atkins, E.T. Adman, 1.3-Å resolution structure of human glutathione *S*-transferase with *S*-hexyl glutathione bound reveals possible extended ligandin binding site, Proteins 48 (2002) 618–627.
[21] A. Vagin, A. Teplyakov, MOLREP: an automated program for molecular replacement, J. Appl. Cryst. 30 (1997) 1022–1025.
[22] G.N. Murshudov, A.A. Vagin, E.J. Dodson, Refinement of macromolecular structures by the maximum-likelihood method, Acta Crystallogr. D53 (1997) 240–255.
[23] T.A. Jones, M. Bergdoll, M. Kjeldgaard, O: a macromolecule modeling environment, in: C.E. Bugg, S.E. Ealick (Eds.), Crystallographic and Modeling Methods in Molecular Design, Springer-Verlag, New York, 1990, pp. 189–195.
[24] N. Guex, M.C. Peitsch, SWISS-MODEL and the Swiss-PdbViewer: an environment for comparative protein modeling, Electrophoresis 18 (1997) 2714–2723.
[25] P. Emsley, K. Cowtan, Coot: model-building tools for molecular graphics, Acta Crystallogr. D60 (2004) 2126–2132.
[26] R.A. Laskowski, J.A.C. Rullmann, M.W. MacArthur, R. Kaptein, J.M. Thornton, AQUA and PROCHECK-NMR: programs for checking the quality of protein structures solved by NMR, J. Biomol. NMR. 8 (1996) 477–486.
[27] E.C. Dietze, C. Ibarra, M.J. Dabrowski, A. Bird, W.M. Atkins, Rational modulation of the catalytic activity of A1-1 glutathione *S*-transferase: evidence for incorporation

of an on-face (pi…HO–Ar) hydrogen bond at tyrosine-9, Biochemistry 35 (1996) 11938–11944.
[28] A.M. Caccuri, M. Lo Bello, M. Nuccetelli, M. Nicotra, P. Rossi, G. Antonini, G. Federici, G. Ricci, Proton release upon glutathione binding to glutathione transferase P1-1: kinetic analysis of a multistep glutathione binding process, Biochemistry 37 (1998) 3028–3034.
[29] C.N. Pace, Determination and analysis of urea and guanidine hydrochloride denaturation curves, Methods Enzymol. 131 (1986) 266–280.
[30] W.H. Habig, W.B. Jakoby, Assays for differentiation of glutathione *S*-transferases, Methods Enzymol. 77 (1981) 398–405.
[31] M. Widersten, R. Björnestedt, B. Mannervik, Involvement of the carboxyl groups of glutathione in the catalytic mechanism of human glutathione transferase A1-1, Biochemistry 35 (1996) 7731–7742.
[32] Y. Sayed, J.A. Hornby, M. Lopez, H. Dirr, Thermodynamics of the ligandin function of human class Alpha glutathione transferase A1-1: energetics of organic anion ligand binding, Biochem. J. 363 (2002) 341–346.
[33] E. Grahn, M. Novotny, E. Jakobsson, A. Gustafsson, L. Grehn, B. Olin, D. Madsen, M. Wahlberg, B. Mannervik, G.J. Kleywegt, New crystal structures of human glutathione transferase A1-1 shed light on glutathione binding and the conformation of the C-terminal helix, Acta Crystallogr. D Biol. Crystallogr. D62 (2006) 197–207.
[34] R.W. Wang, D.J. Newton, A.R. Johnson, C.B. Pickett, A.Y. Lu, Site-directed mutagenesis of glutathione *S*-transferase YaYa. Mapping the glutathione-binding site, J. Biol. Chem. 268 (1993) 23981–23985.
[35] E.T. Adman, I. Le Trong, R.E. Stenkamp, B.S. Nieslanik, E.C. Dietze, G. Tai, C. Ibarra, W.M. Atkins, Localization of the C-terminus of rat glutathione *S*-transferase A1-1: crystal structure of mutants W21F and W21F/F220Y, Proteins 42 (2001) 192–200.
[36] A.M. Caccuri, G. Antonini, P.G. Board, M.W. Parker, M. Nicotra, M. Lo Bello, G. Federici, G. Ricci, Proton release on binding of glutathione to alpha, mu and delta class glutathione transferases, Biochem. J. 344 (1999) 419–425.
[37] A.P. Demchenko, Ultraviolet spectroscopy of proteins, Springer Verlag, Berlin, 1986 pp 21.
[38] S. Liu, P. Zhang, X. Ji, W.W. Johnson, G.L. Gilliland, R.N. Armstrong, Contribution of tyrosine 6 to the catalytic mechanism of isoenzyme 3–3 of glutathione *S*-transferase, J. Biol. Chem. 267 (1992) 4296–4299.
[39] D.F.A.R. Dourado, P.A. Fernandes, B. Mannervik, M.J. Ramos, Glutathione transferase: new model for glutathione activation, Chem. Eur. J. 14 (2008) 9591–9598.
[40] P. Winayanuwattikun, A.J. Ketterman, An electron-sharing network involved in the catalytic mechanism is functionally conserved in different glutathione transferase classes, J. Biol. Chem. 280 (2005) 31776–31782.
[41] P. Bico, C.Y. Chen, M. Jones, J. Erhardt, H. Dirr, Class pi glutathione *S*-transferase: Meisenheimer complex formation, Biochem. Mol. Biol. Int. 33 (1994) 887–892.
[42] M.R. Crampton, A spectroscopic study of the reversible reactions of aromatic nitro-compounds with sulphur bases, J. Chem. Soc. B (1968) 1208–1213.
[43] D.C. Kuhnert, Y. Sayed, S. Mosebi, M. Sayed, T. Sewell, H.W. Dirr, Tertiary interactions stabilise the C-terminal region of human glutathione transferase A1-1: a crystallographic and calorimetric study, J. Mol. Biol. 349 (2005) 825–838.
[44] L.O. Nilsson, M. Edalat, P.L. Pettersson, B. Mannervik, Aromatic residues in the C-terminal region of glutathione transferase A1-1 influence rate-determining steps in the catalytic mechanism, Biochim. Biophys. Acta. 1598 (2002) 199–205.
[45] G. Stenberg, P.G. Board, B. Mannervik, Mutation of an evolutionarily conserved tyrosine residue in the active site of a human class alpha glutathione transferase, FEBS Lett. 293 (1991) 153–155.
[46] J. Miller, Reaction mechanisms in organic chemistry, vol. 8, Elsevier, New York, 1968, pp. 137–179.
[47] W.J. Chen, G.F. Graminski, R.N. Armstrong, Dissection of the catalytic mechanism of enzyme 4–4 of glutathione *S*-transferase with alternative substrates, Biochemistry 27 (1988) 647–654.
[48] A.E. Soffers, J.H. Ploemen, M.J. Moonen, T. Wobbes, B. van Ommen, J. Vervoort, P.J. van Bladeren, I.M. Rietjens, Regioselectivity and quantitative structure–activity relationships for the conjugation of a series of fluoronitrobenzenes by purified glutathione *S*-transferase enzymes from rat and man, Chem. Res. Toxicol. 9 (1996) 638–646.
[49] E.M. van der Aar, T. Bouwman, J.N. Commandeur, N.P. Vermeulen, Structure–activity relationships for chemical and glutathione *S*-transferase-catalysed glutathione conjugation reactions of a series of 2-substituted 1-chloro-4-nitrobenzenes, Biochem. J. 320 (1996) 531–540.
[50] J.J. Ory, L.J. Banaszak, Studies of the ligand binding reaction of adipocyte lipid binding protein using the fluorescent probe 1, 8-anilinonaphthalene-8-sulfonate, Biophys. J. 77 (1999) 1107–1116.
[51] W.R. Kirk, E. Kurian, F.G. Prendergast, Characterization of the sources of protein–ligand affinity: 1-sulfonato-8-(1′)anilinonaphthalene binding to intestinal fatty acid binding protein, Biophys. J. 70 (1996) 69–83.
[52] N. Kinsley, Y. Sayed, S. Mosebi, R.N. Armstrong, H.W. Dirr, Characterization of the binding of 8-anilinonaphthalene sulfonate to rat class Mu GST M1-1, Biophys. Chem. 137 (2008) 100–104.
[53] A. Lartigue, A. Gruez, S. Spinelli, S. Rivière, R. Brossut, M. Tegoni, C. Cambillau, The crystal structure of a cockroach pheromone-binding protein suggests a new ligand binding and release mechanism, J. Biol. Chem. 278 (2003) 30213–30218.
[54] E. Schonbrunn, S. Eschenburg, K. Luger, W. Kabsch, N. Amrhein, Structural basis for the interaction of the fluorescence probe 8-anilino-1-naphthalene sulfonate (ANS) with the antibiotic target MurA, Proc. Natl. Acad. Sci. USA 97 (2000) 6345–6349.
[55] E. Kurian, Solution structure of intestinal fatty acid binding protein complexed with 1-anilinonaphthalene-8-sulfonate: implications for ligand binding, PhD thesis, Mayo Foundation, Rochester, MN. (1998).
[56] J.M. Sturtevant, Heat capacity and entropy changes in processes involving proteins, Proc. Natl. Acad. Sci. USA 74 (1977) 2236–2240.
[57] E. Freire, Thermodynamics of protein folding and molecular recognition, Pure Appl. Chem. 69 (1997) 2253–2261.
[58] V.V. Loladze, D.N. Ermolenko, G.I. Makhatadze, Heat capacity changes upon burial of polar and nonpolar groups in proteins, Protein Sci. 10 (2001) 1343–1352.